

MULTI-VIEW CONSISTENT WOUND SEGMENTATION WITH NEURAL FIELDS

Remi Chierchia^{†*}, Léo Lebrat[†], David Ahmedt-Aristizabal^{†*}, Yulia Arzhaeva^{*},
Olivier Salvado[†], Clinton Fookes[†], Rodrigo Santa Cruz[†]

[†] School of Electrical Engineering & Robotics, Queensland University of Technology, Australia

* Imaging and Computer Vision Group, CSIRO Data61, Australia

Remi.Chierchia@hdr.qut.edu.au, David.Ahmedtaristizabal@data61.csiro.au

Project page: <https://remichierchia.github.io/WoundNeRF/>

ABSTRACT

Wound care is often challenged by the economic and logistical burdens that consistently afflict patients and hospitals worldwide. In recent decades, healthcare professionals have sought support from computer vision and machine learning algorithms. In particular, wound segmentation has gained interest due to its ability to provide professionals with fast, automatic tissue assessment from standard RGB images. Some approaches have extended segmentation to 3D, enabling more complete and precise healing progress tracking. However, inferring multi-view consistent 3D structures from 2D images remains a challenge. In this paper, we evaluate **WoundNeRF**, a NeRF SDF-based method for estimating robust wound segmentations from automatically generated annotations. We demonstrate the potential of this paradigm in recovering accurate segmentations by comparing it against state-of-the-art Vision Transformer networks and conventional rasterisation-based algorithms. The code will be released to facilitate further development in this promising paradigm.

Index Terms— Wound Segmentation, Wound Care, 3D Segmentation, View-consistent Segmentation

1. INTRODUCTION

Chronic wound management continues to pose annual pressure on healthcare systems, particularly affecting aged care facilities and rehabilitation centers [1]. The typical recommendation for wound monitoring and assessment is once every two to four weeks [2], yet treatment cycles may extend considerably when healing is ineffective or clinical delays occur. Previous studies have shown that wound measurements strongly correlate with healing trajectories [3]. Accurate and repeatable measurements are essential for effective prognosis and timely intervention, and digital monitoring platforms offer substantial advantages in streamlining this process [4, 5].

This work was supported by the MRFF Rapid Applied Research Translation grant (RARUR000158), CSIRO AI4M Minimising Antimicrobial Resistance Mission, and Australian Government Training Research Program (AGRTP) Scholarship.

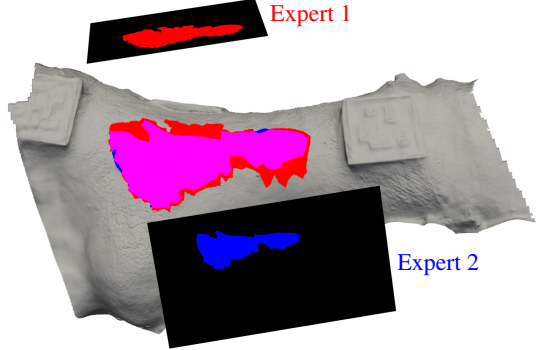


Fig. 1. View inconsistency from mapping 2D expert-annotated masks from different viewpoints onto the underlying 3D surface. Overlapping regions are highlighted in magenta, while non-overlapping regions indicate disagreement.

These platforms compute 3D wound measurements from image data through reconstruction, segmentation, and measurement algorithms. Among these processes, segmentation is crucial, as it identifies the wound and its tissues, defining the regions of the reconstruction to be measured. Despite the inherently three-dimensional characteristics of human anatomy, most existing work focuses on 2D image segmentation [6, 7, 8], encouraged by public initiatives such as the Diabetic Foot Ulcer Challenge (DFUC)¹. However, as anticipated, these frameworks result in limited depth awareness and inconsistencies across viewpoints [9]. We provide a visual representation of this disagreement in Fig. 1.

In this direction, researchers have explored 2D-to-3D semantic fusion algorithms that combine multi-view segmentations to reconstruct 3D estimates [10, 11]. However, these approaches depend on manually tuned heuristics—for instance, considering only camera views whose optical axes remain within a limited angular range of the wound surface normal—which often results in suboptimal segmentation quality. Recent progress in Neural Radiance Fields (NeRFs) [12, 13] provides a promising alternative, enabling joint inference of ap-

¹<https://dfu-challenge.github.io/>

pearance, geometry, and semantics within a single 3D implicit representation that is inherently consistent across viewpoints.

Building on this paradigm, we propose **WoundNeRF**, a method that leverages neural radiance fields to learn a 3D-consistent wound segmentation field directly from multi-view images. In contrast to conventional 2D segmentation or hand-crafted fusion techniques, **WoundNeRF** aggregates pixel-wise semantics across views within a coherent 3D coordinate space. It is important to note that **WoundNeRF**'s primary objective is to learn an optimal aggregation function from automatically generated 2D segmentations, rather than performing a generative task of hallucinating unobserved regions or correcting consistently misclassified areas. We evaluate our approach against fine-tuned Vision Transformer models [14] and 2D-to-3D mapping strategies [11, 15], demonstrating accurate and robust 3D wound segmentation suitable for clinical analysis and digital documentation.

2. METHOD

The **WoundNeRF** architecture consists of a geometry MLP parametrised by a signed distance function (SDF) [12], and a semantic decoder head inspired by [13]. We refer the reader to Fig. 2 for an overview of our method. For conciseness, standard background equations are omitted, and the focus is solely on the segmentation task. The notation used here is consistent with that in previous work [16, 12, 13].

Given a 3D point x , the geometry MLP estimates a feature vector $g(x)$, which is subsequently passed to the semantic head to predict per-class logits across C semantic classes, following the mapping $x \mapsto g(x) \mapsto \mathbf{s}^C(x, g(x))$. Here, \mathbf{s}^C denotes the semantic logits at x , normalised via the *softmax* operation to obtain per-class probabilities.

In our segmentation task, the semantic classes include the background and the following wound bed tissues: granulation, slough, necrotic, and epithelia. We also include an additional wound bed tissue class, termed unknown, to represent wound bed regions without a clear tissue category, maintaining consistency with existing models such as the fine-tuned Vision Transformer from [11]. Thus, the wound bed class (\mathbf{w}) is computed by aggregating the logits of the five wound bed tissues, including unknown:

$$s_{\theta}^{\mathbf{w}}(x, g(x)) = \log \left(\sum_{i=1}^5 \exp(s_{\theta}^i(x, g(x))) \right), \quad (1)$$

where s_{θ}^i denotes the logit for class i . The wound bed probability $\mathbf{s}^{\mathbf{w}}$ is then computed by applying *softmax* to $s_{\theta}^{\mathbf{w}}$ and the background logit s_{θ}^b .

Finally, since the architecture follows the NeRF paradigm, pixel-level predictions are obtained by integrating the semantic distribution over each ray r :

$$\hat{S}^C(r) = \int T(t)\sigma(r(t))\mathbf{s}^C(r(t))dt, \quad (2)$$

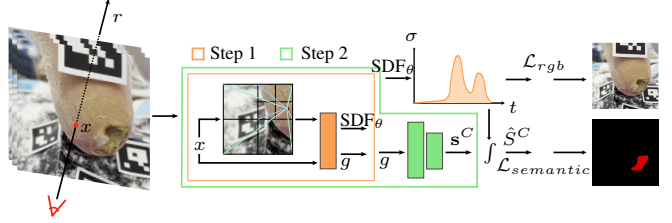


Fig. 2. **WoundNeRF**'s pipeline. For clarity, the explicit dependence on input variables is omitted.

where $T(t)$ denotes the accumulated transmittance along the ray up to depth t , and $\sigma(r(t))$ is the volumetric density at position $(r(t))$.

2.1. Optimization Strategy

The semantic field \mathbf{s}^C is optimised by minimising a weighted cross-entropy loss to address the common class-imbalance problem prevalent in medical imaging [17]:

$$\mathcal{L}_{wce}(r) = -w_{y_r} \log \hat{S}_{y_r}^C(r), \quad (3)$$

where y_r is the ground-truth label for ray r , w_{y_r} is the associated class weight, and $\hat{S}_{y_r}^C(r)$ is the predicted probability of the ground-truth class. It is essential to note that the current formulation enables the integration of alternative segmentation objectives, such as Boundary or Dice loss. For a broader overview of common segmentation losses, we refer readers to [18, 19].

2.2. Implementation Details

The **WoundNeRF** architecture follows *neus-facto* [20] and SemanticNeRF [13] closely. We adopt a two-step strategy where the geometry MLP is first allowed to converge initially, after which the semantic head is activated while the geometry parameters are kept frozen. This strategy stabilises semantic learning by decoupling it from simultaneous geometry optimisation. Class weights used in the weighted cross-entropy loss (Eq. 3) were empirically determined from experiments on a smaller subset of the evaluation dataset.

The background class weight is clipped to 0.1 to reduce its over-representation, while weights for the other classes are assigned proportionally based on their normalised frequencies $w_y = 0.1 + 0.9 * N_y / \sum_{n=1}^5 (N_n)$, where N_i is the total number of pixels across all training images for class i . Given that our method is trained using 2D predictions, which can be inconsistent and inaccurate, we apply *dropout* to the semantic decoder head before the prediction layer with a dropout rate of 0.5. This enforces regularisation, improving robustness and mitigating false positives.

Table 1. Segmentation accuracy across 73 processed videos composing the dataset. The population sizes for wound bed, granulation, and slough classes are 73, 41, and 31, respectively. The symbol \dagger indicates w/o *dropout*.

Method	Wound Bed		Granulation		Slough	
	DSC	Recall	DSC	Recall	DSC	Recall
2D	0.851	0.819	0.738	0.689	0.670	0.609
3D/2D	0.855	0.840	0.761	0.719	0.682	0.614
Ours \dagger	0.851	0.859	0.767	0.764	0.691	0.658
Ours	0.857	0.893	0.775	0.786	0.686	0.666

3. EXPERIMENTS AND RESULTS

We evaluate **WoundNeRF** on a real patient dataset collected in collaboration with clinical researchers. Videos were recorded using consumer-grade devices and processed to extract a set of 50 images per patient following the procedure described in [11]. One to four frames were selected for expert annotation, capturing the wounds from diverse viewing angles to represent their geometric structure.

In our experiments, we compare three methods. The first method, named **2D**, employs a SegFormer [14] MiT-b5 architecture trained on retrospective, real patient data to predict 2D segmentations. The model outputs both a binary segmentation of the wound bed and a multi-class segmentation over five tissue categories. The second method, named **3D/2D**, follows the approach in [11] by aggregating multi-view segmentations predicted by **2D** onto a 3D reconstruction of the scene. The aggregation is performed by projecting the 3D mesh onto 2D segmentation masks via rasterisation and assigning vertex labels based on a weighted majority vote that reflects the reliability of each viewing angle relative to the wound’s surface normal. For quantitative evaluation, these 3D segmentations are back-projected onto 2D views corresponding to expert-annotated ground-truth frames.

Evaluation metrics reported include the Dice Similarity Coefficient (DSC) and Recall. The choice of these metrics reflects considerations on their widespread use and the quality of the ground-truth annotations. The evaluation dataset comprises 73 videos from 35 patients, featuring diverse wound recordings. It includes longitudinal recordings of wounds, multiple wounds per patient, and various recordings within a single assessment. This dataset was collected as part of a clinical study and does not follow a structured acquisition protocol, reflecting real-world clinical variability. Notably, the necrotic and epithelial tissue classes are under-represented in the dataset and are therefore omitted from the reported results.

Accuracy Evaluation. The first evaluation assessed the accuracy of the predicted masks for the wound bed and tissue classes, as reported in Table 1. Our method consistently improves upon both comparison methods across all metrics and

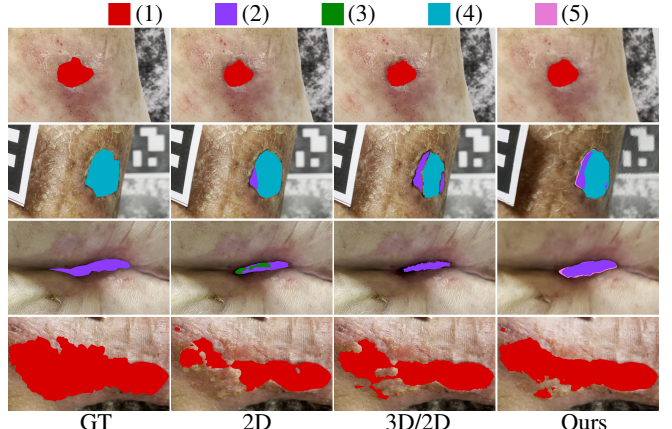


Fig. 3. Qualitative comparison of segmentation masks across the compared methods for four wounds. Our method additionally renders the learned RGB appearance, visible in the background region with a subtle colour tint and slightly reduced sharpness. The top and bottom rows display wound bed (1) masks, while the middle rows represent the two most common tissue classes, granulation (2) and slough (4), respectively. The necrotic (3) and unknown (5) tissue classes are also displayed, except for the epithelial class.

classes, with notable improvements in tissue classification.

While these quantitative metrics summarise average performance across the dataset, they do not fully capture the quality of the predictions. Fig. 3, provides a visual comparison of the predicted masks. Notably, our method generally predicts smoother boundaries (first row of the figure) and achieves higher recall. This reflects the technical benefits of learning a semantic field in a 3D-consistent fashion that implicitly enforces spatial coherence. Specifically, in the second row of the figure, the **3D/2D** method fails to recover a smooth transition between labels, resulting in segmented wound bed regions that appear disjointed. In contrast, our method learns spatial correlations within the semantic field, providing visually improved masks. Notably, this enables more accurate measurement of wound metrics such as size and area, which are critical for clinical wound documentation [3].

In the third row, our method effectively mitigates errors present in the **2D** tissue predictions, enhancing tissue coverage. The pink region represents the unknown class, which we include within the wound bed region in our analysis.

Finally, the bottom row illustrates a challenging scenario commonly encountered in the dataset, where segmentation masks can be sparse and inconsistent. Despite these challenges, our method achieves significantly better wound bed segmentation compared to other approaches.

Robustness. To evaluate robustness to errors in the training masks, we conducted experiments that simulated mask boundary perturbations, as detailed in Table 2. Specifically,

Table 2. Robustness evaluation of segmentation methods across the 73 processed videos. The wound bed population size is 73 for all perturbation experiments.

Method	Perturbation	Wound Bed	
		DSC	Recall
2D	Erosion-Dilation	0.816	0.751
3D/2D	Erosion-Dilation	<u>0.834</u>	<u>0.792</u>
Ours	Erosion-Dilation	0.835	0.887
2D	Jittering	0.798	0.722
3D/2D	Jittering	<u>0.824</u>	<u>0.772</u>
Ours	Jittering	0.835	0.878
3D/2D	Half the frames	0.848	0.831
Ours	Half the frames	0.850	0.886

we applied random erosion and dilation perturbations with a radius of 3 pixels (Erosion-Dilation in the table) to simulate common scenarios where 2D segmentation methods exhibit under- or over-confidence. Additionally, we introduced a boundary jitter perturbation (Jittering in the table), which randomly flips pixel values within a 3-pixel boundary region. Although less realistic, this perturbation significantly affects the comparison methods, whereas our NeRF-based architecture exhibits only a minimal performance degradation.

These experiments confirm the presence of inherent errors introduced by 2D segmentations and underscore the necessity for view-consistent segmentation approaches. Our results indicate that all methods are more sensitive to random pixel perturbations near mask boundaries than to noise that is correlated among neighbouring pixels. Additionally, both **2D** and **3D/2D** methods exhibit a considerable drop in recall, resulting in consistent underestimation of wound size, which may limit clinical applicability. In contrast, our method demonstrates consistent performance with a notably smaller drop in recall, highlighting the implicit spatial regularisation of correlations via the NeRF paradigm.

Another experiment investigated the effect of reducing the number of training images from the original 50 to 25 frames (Half the frames in the table). This reduction impacts both methods equally and is less severe than the boundary perturbations, while our method maintains superior accuracy.

4. DISCUSSION

Analysis of the experimental results indicates that our method offers advantages in both accuracy and robustness, particularly by demonstrating superior aggregation of multi-view 2D segmentations compared to the **3D/2D** approach. However, its performance is constrained by the quality of the training images, leading to suboptimal learning outcomes as illustrated in the bottom row of Fig. 3. Such scenarios are likely to occur frequently in real-world applications, highlighting

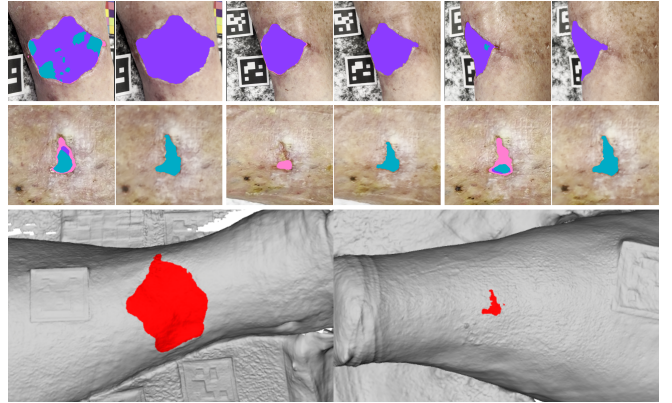


Fig. 4. Qualitative comparison **2D** predictions versus our method trained with few views. The first two rows present three different views, showing the **2D** predictions on the left and renderings produced by our method on the right. The bottom row displays the corresponding wound segmentation on the 3D mesh extracted from our method.

promising directions for future research.

Automatic wound segmentation is enabled by architectures such as SegFormer [14], which have significantly advanced the accessibility of unsupervised segmentation methods. In particular, the availability of large annotated datasets is often scarce, potentially limiting fine-tuning strategies. To address this, we trained our model using only expert-annotated masks from a subset containing between two and four ground-truth views. From this model, we generated predictions for 50 unseen viewpoints and qualitatively compared them to those from the **2D** model. As shown in Fig. 4, **2D** predictions exhibit high inconsistency and noise, frequently containing multiple tissue classes. Notably, in the second row, three similar views display considerable variance. In contrast, our method maintains consistency across views by learning a semantic field directly in 3D space, thereby opening opportunities for data augmentation to enhance the training of automatic 2D segmentation models.

Furthermore, our method captures the underlying 3D geometry, enabling mesh extraction to facilitate automatic wound documentation. An example visualisation of a reconstructed wound rendered in 3D and inpainted with the learned segmentation field is shown in the bottom row of Fig. 4.

5. CONCLUSION

We presented **WoundNeRF**, a method for producing multi-view consistent wound segmentations. Our approach overcomes the limitations of 2D segmentations, which often fail to capture the full 3D topology of wounds, by aggregating information across multiple views to generate more accurate and coherent wound segmentations. Although **WoundNeRF** improves segmentation consistency, it still faces challenges

with misclassified pixels. Future research will integrate a confidence-driven segmentation framework to enhance robustness and further improve the semantic fidelity of wound representations for clinical applications.

6. COMPLIANCE WITH ETHICAL STANDARDS

This study was performed in line with the principles of the Declaration of Helsinki. The experimental procedures involving human subjects described in this paper were approved by the CSIRO Health and Medical Human Research Ethics Committee, the University of Sydney, and the Greater Western Human Research Ethics Committees [Ethics protocol number: 2022/HE000523; 2022/HE000820; 2023/ETH01164; 2023/HE000916].

7. ACKNOWLEDGMENTS

The authors would like to acknowledge Hayley Ryan and WoundRescue Pty Ltd, who supported the development of the retrospective clinical wound dataset, the collection of wound images, and image annotations. Ms Joanne Marjoram and Ms Cassandra Kelly, clinical nurse researchers at the University of Sydney School of Rural Health, for facilitating and conducting the collection of chronic wound images for the prospective data. We also thank A/Prof. Georgina Luscombe for leading the ethical approvals, data assessment and validation, and the review of user requirements; Ms Kate Smith for research ethics and governance support; and Dr Annie Banbury and Ms Melanie Pefani, Coviu Global Pty Ltd., for assistance with image annotation and the development and review of user requirements.

8. REFERENCES

- [1] Laura Martinengo, Maja Olsson, Ram Bajpai, Michael Soljak, Zee Upton, Artur Schmidtchen, Josip Car, and Krister Järbrink, “Prevalence of chronic wounds in the general population: systematic review and meta-analysis of observational studies,” *Annals of epidemiology*, vol. 29, pp. 8–15, 2019.
- [2] M Flanagan, “Wound measurement: can it help us to monitor progression to healing?,” *Journal of wound care*, vol. 12, no. 5, pp. 189–194, 2003.
- [3] Junko Sugama, Yuko Matsui, Hiromi Sanada, Chizuko Konya, Mayumi Okuwa, and Atsuko Kitagawa, “A study of the efficiency and convenience of an advanced portable wound measurement system (visitraktm),” *Journal of clinical nursing*, vol. 16, no. 7, pp. 1265–1269, 2007.
- [4] Angela Christine Chang, Bronwyn Dearman, and John Edward Greenwood, “A comparison of wound area measurement techniques: visitrak versus photography,” *Eplasty*, vol. 11, pp. e18, 2011.
- [5] Dhanesh Ramachandram, Jose Luis Ramirez-GarciaLuna, Robert DJ Fraser, Mario Aurelio Martínez-Jiménez, Jesus E Arriaga-Caballero, Justin Allport, et al., “Fully automated wound tissue segmentation using deep learning on mobile devices: Cohort study,” *JMIR mHealth and uHealth*, vol. 10, no. 4, pp. e36977, 2022.
- [6] Chuanbo Wang, DM Anisuzzaman, Victor Williamson, Mriyal Kanti Dhar, Behrouz Rostami, Jeffrey Niezgoda, Sandeep Gopalakrishnan, and Zeyun Yu, “Fully automatic wound segmentation with deep convolutional neural networks,” *Scientific reports*, vol. 10, no. 1, pp. 21897, 2020.
- [7] Changhan Wang, Xinchen Yan, Max Smith, Kanika Kochhar, Marcie Rubin, Stephen M Warren, James Wrobel, and Honglak Lee, “A unified framework for automatic wound segmentation and analysis with deep convolutional neural networks,” in *2015 37th annual international conference of the ieee engineering in medicine and biology society (EMBC)*. IEEE, 2015, pp. 2415–2418.
- [8] Huimin Lu, Bin Li, Junwu Zhu, Yujie Li, Yun Li, Xing Xu, Li He, Xin Li, Jianru Li, and Seiichi Serikawa, “Wound intensity correction and segmentation with convolutional neural networks,” *Concurrency and computation: practice and experience*, vol. 29, no. 6, pp. e3927, 2017.
- [9] Damir Filko, Robert Cupec, and Emmanuel Karlo Nyarko, “Wound measurement by RGB-D camera,” *Mach. Vis. Appl.*, vol. 29, pp. 633–654, 2018.
- [10] Rania Niri, Evelyn Gutierrez, Hassan Douzi, Yves Lucas, Sylvie Treuillet, Benjamín Castañeda, and Ivan Hernandez, “Multi-view data augmentation to improve wound segmentation on 3D surface model by deep learning,” *IEEE Access*, vol. 9, pp. 157628–157638, 2021.
- [11] Remi Chierchia, Rodrigo Santa Cruz, Léo Lebrat, Yulia Arzhaeva, Mohammad Ali Armin, Jeremy Oorloff, Chuong Nguyen, Olivier Salvado, Clinton Fookes, and David Ahmedt-Aristizabal, “Wound3dassist: A practical framework for 3d wound assessment,” *arXiv preprint arXiv:2508.17635*, 2025.
- [12] Peng Wang, Lingjie Liu, Yuan Liu, Christian Theobalt, Taku Komura, and Wenping Wang, “Neus: Learning neural implicit surfaces by volume rendering for multi-view reconstruction,” *NeurIPS*, 2021.
- [13] Shuaifeng Zhi, Tristan Laidlow, Stefan Leutenegger, and Andrew J. Davison, “In-place scene labelling and understanding with implicit scene representation,” in *Proceedings of the IEEE/CVF International Conference on Computer Vision (ICCV)*, October 2021, pp. 15838–15847.
- [14] Enze Xie, Wenhui Wang, Zhiding Yu, et al., “SegFormer: Simple and efficient design for semantic segmentation with transformers,” *Adv. Neural Inf. Process. Syst.*, vol. 34, pp. 12077–12090, 2021.
- [15] Léo Lebrat, Rodrigo Santa Cruz, Remi Chierchia, Yulia Arzhaeva, Mohammad Ali Armin, Joshua Goldsmith, Jeremy Oorloff, Prithvi Reddy, Chuong Nguyen, Lars Petersson, et al., “Syn3dwound: a synthetic dataset for 3d wound bed analysis,” in *2024 IEEE International Symposium on Biomedical Imaging (ISBI)*. IEEE, 2024, pp. 1–5.
- [16] Ben Mildenhall, Pratul P Srinivasan, Matthew Tancik, Jonathan T Barron, Ravi Ramamoorthi, and Ren Ng, “Nerf:

Representing scenes as neural radiance fields for view synthesis,” *Communications of the ACM*, vol. 65, no. 1, pp. 99–106, 2021.

- [17] Michael Yeung, Evis Sala, Carola-Bibiane Schönlieb, and Leonardo Rundo, “Unified focal loss: Generalising dice and cross entropy-based losses to handle class imbalanced medical image segmentation,” *Computerized Medical Imaging and Graphics*, vol. 95, pp. 102026, 2022.
- [18] Jun Ma, Jianan Chen, Matthew Ng, Rui Huang, Yu Li, Chen Li, Xiaoping Yang, and Anne L Martel, “Loss odyssey in medical image segmentation,” *Medical image analysis*, vol. 71, pp. 102035, 2021.
- [19] Reza Azad, Moein Heidary, Kadir Yilmaz, Michael Hüttemann, Sanaz Karimijafarbigloo, Yuli Wu, Anke Schmeink, and Dorit Merhof, “Loss functions in the era of semantic segmentation: A survey and outlook,” *arXiv preprint arXiv:2312.05391*, 2023.
- [20] Zehao Yu, Anpei Chen, Bozidar Antic, Songyou Peng, Apratim Bhattacharyya, Michael Niemeyer, Siyu Tang, Torsten Satler, and Andreas Geiger, “Sdfstudio: A unified framework for surface reconstruction,” 2022.